

Modeling, Identification and Control of Model Jet Engines for Jet Powered Robotics

Giuseppe L'Erario¹, Luca Fiorio¹, Gabriele Nava^{1,2}, Fabio Bergonti¹,
Hosameldin Awadalla Omer Mohamed¹, Silvio Traversaro¹ and Daniele Pucci¹

Abstract—The paper contributes towards the modeling, identification, and control of model jet engines. We propose a nonlinear, second order model in order to capture the model jet engines governing dynamics. The model structure is identified by applying sparse identification of nonlinear dynamics, and then the parameters of the model are found via gray-box identification procedures. Once the model has been identified, we approached the control of the model jet engine by designing two control laws. The first one is based on the classical Feedback Linearization technique while the second one on the Sliding Mode control. The overall methodology has been verified by modeling, identifying and controlling two model jet engines, i.e. P100-RX and P220-RXi developed by JetCat, which provide a maximum thrust of 100 N and 220 N, respectively.

I. INTRODUCTION

Flying vehicles are not new to the Robotics community. Quadrotors, tail-sitters, and scale airplanes are only few examples of the large variety of existing flying robots [1]. Yet, despite decades of research in the subject, the current propulsion systems for aerial robots still enables only flight of relatively light vehicles. This paper takes a first step towards the modeling and control of model jet engines having high thrust-to-weight ratios. It thus paves the way to Jet Powered Robotics, and enables the design of flying robots that may then be endowed with additional functionalities than the current state-of-the-art flying robotic platforms.

Flying robots possess the capacity of aerial locomotion. When attempting at augmenting this capacity with a degree of manipulation or locomotion, flying robots soon become heavier and more complex to control. For instance, aerial locomotion and manipulation have been combined by *Aerial Manipulation* [2], a branch of robotics often exemplified by a quadrotor equipped with a robotic arm [3]. In this case, the robotic arm attached to the flying robot is often required to meet strict requirements on its weight, thus limiting the interaction capability of the aerial manipulator.

Aerial and terrestrial locomotion have also been combined in single robotic platforms. These robots exhibit multimodal locomotion capabilities [4], [5], [6], [7], [8], i.e. they can fly and move on the ground by using contacts. Multimodal robots are more energetically efficient than classical aerial vehicles, but they share the same drawback: a very limited interaction ability with the environment. So, it is tempting

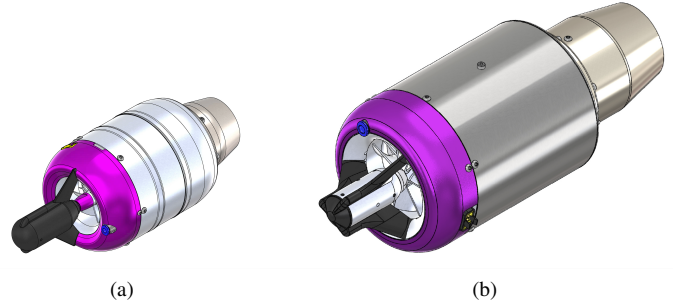


Fig. 1: The model jet engines used for the experimental analysis: The P100-RX (a) and the P220-RXi (b) developed by JetCat.

to complement multimodal robots with a degree of manipulation, but the current electric propulsion system is still a barrier for such an augmentation.

Recently, attempts at combining aerial and bipedal terrestrial locomotion have also attracted the attention of the robotics community. LEg ON Aerial Robotic DrOne, or Leonardo, at the Caltech's Center for Autonomous Systems and Technologies (CAST) combines two robotic legs with two propellers to improve balancing and agility [9]. Analogously, at Guangdong University of Technology's School of Automation, researchers are developing a legged robot with ducted fans installed at the feet. The goal is to allow the robot to take larger steps [10]. Yet, none of these robots is endowed with a degree of manipulation.

An attempt at unifying manipulation, aerial, and bipedal terrestrial locomotion on a single robotic platform is given by the iRonCub project, whose aim is to make the humanoid robot iCub fly [11], [12], [13]. For such applications, where the propulsion system has to provide enough thrust to lift a complete humanoid robot, electric ducted fans are no longer suitable. An option is then to choose high thrust-to-weight ratio propulsion systems, as *model jet engines* – see Fig. 1.

Despite the vast literature on aircraft jet engines [14], modeling, identification, and control of model jet engines are lagging behind, mostly because their application to Robotics is still at the embryonic stage. Several textbooks address the jet engine design in detail, starting from the working cycle, internal systems, and performance including maintenance [15]. But there is still no application of these advanced techniques to model jet engines. The application of these advanced techniques, however, would require precise and

¹Dynamic Interaction Control research line of Fondazione Istituto Italiano di Tecnologia, via Morego 30, Genoa, Italy. Email addresses: `firstname.surname@iit.it`, `hosameldin.mohamed@iit.it`

²DIBRIS, University of Genova, Genova, Italy.

Robot weight [kg] \ Flight time [min]	1	3	5
10	0.86	3.12	6.57
20	1.72	6.25	13.15
30	2.58	9.37	19.73
40	3.44	12.50	26.31
50	4.31	15.62	32.89

(a) Electric propulsion.

Robot weight [kg] \ Flight time [min]	1	3	5
10	0.22	0.67	1.15
20	0.44	1.35	2.30
30	0.66	2.02	3.45
40	0.88	2.70	4.61
50	1.10	3.38	5.76

(b) Jet propulsion.

Fig. 2: The weight in kg of the battery bank in case of electric propulsion (a). The weight in kg of fuel in case of jet propulsion (b).

numerous information about the model jet engine, like the internal geometry, the fuel heating value, use condition, air density etc. These information may not be always available, and alternative and experimental based methods shall be developed to circumvent these modelling difficulties.

This paper takes the first step for enabling the use of model jet engines in robotics applications. More precisely, the manuscript presents modelling, identification, and control techniques for model jet engines, and performs experimental validation of the proposed methods. To the best of the authors knowledge, the paper is the first comprehensive treatment of model jet engines, ranging from modeling to experimental validation. In particular, concerning modeling and identification, the contribution of the paper is twofold. Starting from experimental data, we first use the sparse identification of nonlinear dynamics SINDy [16] in order to find out the governing jet engine model. After fixing the model structure, we perform *grey-box* estimation using two methods: batch least squares and recursive extended Kalman Filter. The overall modelling and identification procedure outcomes the model then used in the control design. We tackle the control of the model jet engines by applying and comparing *feedback linearization* and *sliding mode* control [17], [18]. The overall approach presented in the paper is verified experimentally on the model jet engines P100-RX and P220-RXi developed by JetCat. These experimental activities are carried out in a dedicated setup that has been designed and built for the purpose of this manuscript.

The paper is organized as follows. Section II motivates the use of model jet engines in robotics. Section III recalls the extended Kalman filter algorithm and provides a simple example for the Sliding mode controller. Section IV describes the test bench and the hardware used for the experimental analysis. In the Section V the identification procedure is illustrated and the results are validated. Section VI deals with the control architecture used on the jet engines and the relative experimental results. Conclusions and perspectives conclude the paper in Section VII.

II. WHY JET POWERED ROBOTICS

Electric propulsion systems are nowadays the common actuators for flying robots. The relative simplicity in using brushless and brushed motors, and the advent of efficient and strong propellers paved the way to flying robots powered by electric propulsion. One of the drawbacks of electric powered flying robots is clearly the need of high power, and consequently large capacity batteries, when the robot weight increases considerably. In these cases, model jet engines, which are much more efficient in terms of thrust to weight ratios, may be a solution for heavy flying robots.

For the purpose of understanding when model jet engines should be preferred to electrical motors, we consider the problem of making a robot – of a given weight – hover for a specific amount of time. Then, we estimate the associated weight of LiPo battery banks and jet fuel in the electrical and jet engine case, respectively. We assume that the specific energy density of the LiPo batteries is 210 Wh/kg [19], and that the density of the jet fuel (i.e. diesel) is 0.8 kg/l [20].

More specifically, the analysis is carried out considering the performances of the following two propulsion systems:

- **Dynamax CAT 6 FAN** [21], an electric motor with a maximum thrust of ~ 13 kg at ~ 13 kW consumption;
- **JetCat P220-RXi** [22], a model jet engine with maximum thrust of ~ 22 kg at ~ 0.6 l/min consumption;

We also assume that energy and fuel consumption are linear versus the generated thrust, and that the engine weights are neglectable. The tables in Figure 2 show the difference in terms of weight that is needed to power the robot for the electric and jet engine case, respectively. If we consider, for instance, a 40 Kg robot performing five minute flight, the advantage of using model jet engines is evident: we would need 26.31 Kg of battery pack versus 4.61 Kg of fuel. This specific considered case is that of the envisaged flying version of the humanoid robot iCub.

Another interesting element of comparison is the number of engines needed to lift a specific weight. Table I shows this comparison, and we observe that a 40 Kg robot performing hovering needs 4 electrical motors instead only 2 jet turbines.

TABLE I: Number of engines needed for hovering.

Robot weight [kg]	10	20	30	40	50
Electrical prop.	1	2	3	4	4
Jet prop.	1	1	2	2	3

III. BACKGROUND

A. Notation

- $\mathbf{a} \in \mathbb{R}^i$ is a vector of dimension i ;
- $\mathbf{A} \in \mathbb{R}^{i \times j}$ is a matrix of size $i \times j$;
- $\mathbf{x} \in \mathbb{R}^n$ is the state vector of a generic system;
- $\mathbf{u} \in \mathbb{R}^p$ is the input vector of a generic system;
- $\mathbf{y} \in \mathbb{R}^m$ is the output vector of a generic system;
- $\mathbf{z} \in \mathbb{R}^m$ is the measurement vector;
- $[T, \dot{T}]^\top \in \mathbb{R}^2$ is the state vector of the jet engine model;
- $T \in \mathbb{R}^1$ is the thrust of the jet engine model;
- $u \in \mathbb{R}^1$ is the input of the jet engine model, namely the *PWM*;

B. Recall on Kalman Filter

We briefly recall here the formulation of the discrete Extended Kalman filter [23], Sec. 13.2.3.

The Kalman Filter (KF) is a recursive filter that estimates the state of a linear system from a series of noisy measurements \mathbf{z} . In particular, consider a discrete nonlinear system:

$$\mathbf{x}_{k+1} = f(\mathbf{x}_k, \mathbf{u}_k) + \mathbf{w}_k \quad (1a)$$

$$\mathbf{y}_k = h(\mathbf{x}_k) + \mathbf{v}_k \quad (1b)$$

subject to process noise \mathbf{w}_k and measurement noise \mathbf{v}_k . The noises are uncorrelated, zero mean Gaussian noises and have known covariance matrices $\mathbf{Q}_k \in \mathbb{R}^{n \times n}$ and $\mathbf{R}_k \in \mathbb{R}^{m \times m}$ describing the process and the measurement noise, respectively.

The covariance of the estimation error \mathbf{P}_k is defined as:

$$\mathbf{P}_k = E[(\mathbf{x}_k - \hat{\mathbf{x}}_k)(\mathbf{x}_k - \hat{\mathbf{x}}_k)^\top] \quad (2)$$

with $\mathbf{P}_k \in \mathbb{R}^{n \times n}$, \mathbf{x}_k and $\hat{\mathbf{x}}_k$ the true state and its estimation, and $E(\cdot)$ the operator denoting the expected value.

The Extended Kalman Filter uses Taylor series to expand the nonlinear system equations around the current state estimate with partial derivatives:

$$\mathbf{F}_k = \left. \frac{\partial f}{\partial \mathbf{x}} \right|_{\hat{\mathbf{x}}_k}, \quad \mathbf{H}_k = \left. \frac{\partial h}{\partial \mathbf{x}} \right|_{\hat{\mathbf{x}}_k} \quad (3)$$

Since the system is now linear, we can use the standard Kalman filter equation for state estimation. The extended Kalman filter procedure is briefly described in algorithm 1.

C. Recall on Sliding Mode controller

Sliding Mode Control is a classical robust control technique [18]. The underlying idea is to force the system trajectories to converge to a *sliding manifold*, where the system evolution is independent from the model uncertainties.

A main drawback of Sliding mode control is the so called *chattering*, which often excites unmodeled high-frequency dynamics, thus degrading the overall system performance.

Algorithm 1 discrete-time extended Kalman Filter

1: Initialization:

$$\hat{\mathbf{x}}_0 = E(\mathbf{x}_0)$$

$$\mathbf{P}_0 = E[(\mathbf{x}_0 - \hat{\mathbf{x}}_0)(\mathbf{x}_0 - \hat{\mathbf{x}}_0)^\top]$$

2: **for** $k = 1, 2, \dots, N$ **do** $\triangleright N = \text{experiment length}$

3: Compute the (process) partial derivative matrix:

$$\mathbf{F}_{k-1} = \left. \frac{\partial f}{\partial \mathbf{x}} \right|_{\hat{\mathbf{x}}_{k-1}} \quad \mathbf{L}_{k-1} = \left. \frac{\partial f}{\partial \mathbf{u}} \right|_{\hat{\mathbf{u}}_{k-1}}$$

4: Project the state and the error covariance:

$$\hat{\mathbf{x}}_k = f(\mathbf{x}_{k-1}, \mathbf{u}_{k-1})$$

$$\mathbf{P}_k = \mathbf{F}_{k-1} \mathbf{P}_{k-1} \mathbf{F}_{k-1}^\top + \mathbf{L}_{k-1} \mathbf{Q}_{k-1} \mathbf{L}_{k-1}^\top$$

5: Compute the (observation) partial derivative matrix:

$$\mathbf{H}_k = \left. \frac{\partial h}{\partial \mathbf{x}} \right|_{\hat{\mathbf{x}}_k} \quad \mathbf{M}_k = \left. \frac{\partial h}{\partial \mathbf{u}} \right|_{\hat{\mathbf{u}}_k}$$

6: Compute the Kalman gain:

$$\mathbf{K}_k = \mathbf{P}_k \mathbf{H}_k^\top (\mathbf{H}_k \mathbf{P}_k \mathbf{H}_k^\top + \mathbf{M}_k \mathbf{R}_k \mathbf{M}_k^\top)^{-1}$$

7: Update the state $\hat{\mathbf{x}}_k$ and the error covariance \mathbf{P}_k incorporating the measurement \mathbf{z}_k

$$\hat{\mathbf{x}}_k \leftarrow \hat{\mathbf{x}}_k + \mathbf{K}_k (\mathbf{z}_k - h(\hat{\mathbf{x}}_k))$$

$$\mathbf{P}_k \leftarrow (\mathbf{I} - \mathbf{K}_k \mathbf{H}_k) \mathbf{P}_k$$

The following lemma recalls an application of the Sliding mode control combined with a technique commonly used to reduce chattering.

Lemma 1 ([18], Sec. 14.1). *Consider the second-order system:*

$$\dot{x}_1 = x_2 \quad (4a)$$

$$\dot{x}_2 = f(\mathbf{x}) + g(\mathbf{x})u \quad (4b)$$

where $f(\mathbf{x})$ and $g(\mathbf{x})$ are uncertain nonlinear functions and $g(\mathbf{x}) > 0$, $\forall \mathbf{x} \in \mathbb{R}^2$.

Assuming that:

- $\hat{f}(\mathbf{x})$ and $\hat{g}(\mathbf{x})$ represent the nominal model;
- $\beta(\mathbf{x})$ is an upper bound on the perturbation term;

the control law:

$$u = - \underbrace{\frac{a_1 x_2 + \hat{f}(\mathbf{x})}{\hat{g}(\mathbf{x})}}_{\text{continuous component}} - \underbrace{\frac{\beta(\mathbf{x}) \cdot \text{sgn}(s)}{\beta(\mathbf{x})}}_{\text{switching component}} \quad (5)$$

constraints the motion of the system on the so called sliding manifold

$$s = a_1 x_1 + x_2 = 0$$

On this manifold, the motion is governed by $\dot{x}_1 = -a_1 x_1$. If $a_1 > 0$, $\mathbf{x}(t)$ tends to zero. The constant a_1 also regulates the rate of convergence to this manifold. More details on the Sliding mode control can be found in [18].

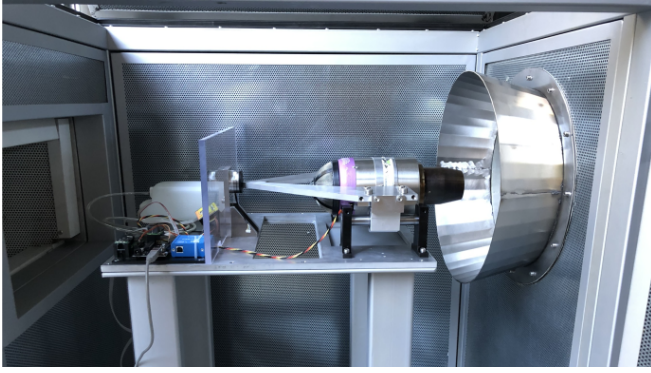


Fig. 3: The setup used for jet experimental campaigns.

IV. THE TEST BENCH FOR JET EXPERIMENTAL ACTIVITIES

Carrying out experimental activities with jet turbines is not a straightforward activity. Exhaustion gas at about 800° Celsius, flammable fuel, and rotating turbines at about 200000 RPMs are only few challenges that, if not dealt with carefully, may turn to be hazardous for the staff conducting the experimental campaigns. In this section, we describe the setup of model jet turbines that was designed and built to secure the experimental activities presented in this paper.

First, the setup had to be compatible with two types of model jet engines: the P100-RX and the P220-RXi by JetCat [24], [22]. Each turbine comes with a dedicated Electronic Control Unit (ECU) and a Ground Support Unit (GSU). The ECU can work through two different communication interfaces: throttle and serial. The throttle interface is the most basic one, and accepts a Pulse With Modulation (PWM) input signal to regulate the turbine thrust. The serial interface receives the desired throttle as a message, but can also send a feedback message that details the running status of the engine. The default engine fuel is kerosene Jet-A1, but the performances are similar also if diesel is used. The main characteristics of the two engines are in Table II.

The turbines, due to their dangerous nature, required the design and construction of a dedicated protecting case. Fig. 3 depicts the interior of the turbine case. Starting from the left we have the air intake opening, the turbine instrumentation and the exhaust cone. Furthermore, the case has been designed to be explosion and fire proof.

As depicted in Fig. 4, the turbine instrumentation consists in a custom designed calibration device and support electronics. More precisely, the calibration device features a V-shaped frame, supported by linear bearings, to which the

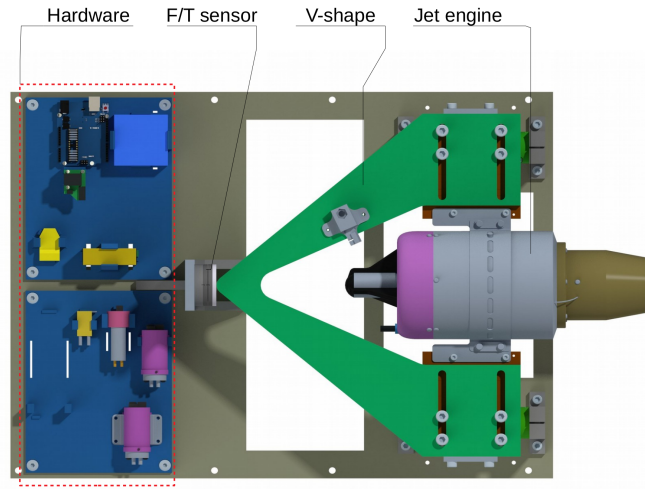


Fig. 4: The hardware scheme. The custom designed instrumentation. On the left side the electronics and pump support plate, while in green the “V-shape” support for the turbines.

jet engines are anchored. The turbine thrust is measured by a 6 axis force torque sensor (F/T) in contact with the V-shaped frame. For what concerns the support electronics, we used an “Arduino-like” board to generate the PWM signal for the throttle interface of the ECU and a USB-CAN box to read the F/T measurements.

Both the board and the box were connected through a USB port to a laptop running YARP [25] and a MATLAB/Simulink controller. The communication between the support electronics was implemented by using YARP devices and ports, while the communication between YARP and the controller was implemented through the Whole-Body Toolbox [26]. The whole control architecture was running at a frequency of 100 Hz.

V. MODELING AND IDENTIFICATION OF JET TURBINES

The test bench presented in Sec. IV can be used to collect input (throttle) and output (thrust) data. A typical dataset collected during an experimental campaign is depicted in Fig. 5. From a qualitative investigation of this picture, it is clear that that second order models for the model jet engine may be good initial candidates for performing *grey-box* identification.

A. Identification of jet model structure

To obtain quantitative evidence of this indication, we applied sparse identification of nonlinear dynamics SINDy [16], which is a state-of-the-art technique to find nonlinear functions describing the relationships between variables and measured dynamics. More precisely, assume that the thrust dynamics is characterised by:

$$\ddot{T} = f(T, \dot{T}, u) \quad (6)$$

where we have only the direct measurements of the thrust T , and \dot{T} and \ddot{T} are retrieved using the Savitzky–Golay filter.

Jet engine model	P100-RX	P220-RXi
Nominal Max. Thrust	100 N	220 N
Throttle range	25% – 100%	25% – 100%
Weight	1080 g	1850 g
Length	241 mm	307 mm
Diameter	97 mm	116.8 mm

TABLE II: Basic specifics of the jet engines.

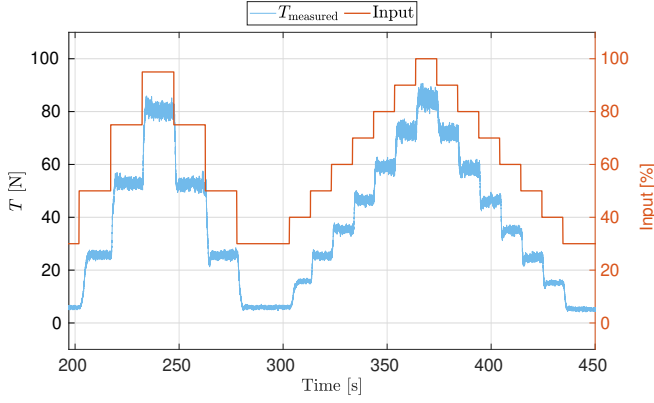


Fig. 5: An example of the dataset we collected during the experimental campaign. The jet turbine is the P100-RX.

The application of the sparse optimization yields [16] :

$$\begin{aligned} \ddot{T} = & a_1 + a_2 T + a_2 T^2 + a_3 \dot{T} + a_4 T \dot{T} + a_5 \dot{T}^2 \\ & + a_6 u + a_7 T u + a_8 \dot{T} u + a_9 u^2, \end{aligned}$$

with also an estimate of the coefficients a_i . Let us observe that the terms depending on the control input u are very sensitive to the tuning parameters of SINDy. This suggests that the nonlinearities depending on the control input u do not play a pivotal role for identification purposes. Then, we decide to fix the model shape so as the resulting nonlinear dynamics is affine with respect to the control input u , i.e.

$$\ddot{T} = f(T, \dot{T}) + g(T, \dot{T}) v(u) \quad (7)$$

where

$$\begin{aligned} f(T, \dot{T}) = & K_T T + K_{TT} T^2 + K_D \dot{T} + \\ & + K_{DD} \dot{T}^2 + K_{TD} T \dot{T} + c \\ g(T, \dot{T}) = & B_U + B_T T + B_D \dot{T} \\ v(u) = & u + B_{UU} u^2 \end{aligned}$$

and u the jet engine input. The model (7) is particularly handy for identification and control purposes presented next.

B. Gray-box identification of the jet model

Once the model (7) is fixed, the objective of gray box identification procedures is to estimate its parameters. Define the parameter vector

$$\mathbf{p} = (K_T, K_{TT}, K_D, K_{DD}, K_{TD}, c, B_U, B_T, B_D, B_{UU})^\top \quad (8)$$

where every element of the vector is a scalar. Then, the goal of the gray box identification is to estimate the vector \mathbf{p} .

The model (7) may be expressed linearly versus \mathbf{p} when linearised. So, one may attempt at identifying the set of parameters by performing a set of experimental activities from which \dot{T}, \ddot{T} are estimated via non causal filters (e.g. Savitzky–Golay) and the set of parameters \mathbf{p} extracted using classical iterative linear regression. The application of this method – whose results are shown in the next section – turned to be not robust with respect to measurement noise.

Another approach to parameter estimation is that of including the parameters \mathbf{p} in an Extended Kalman Filter (EKF), which iteratively estimates the set of parameters \mathbf{p} . More precisely, we can define a generic system so as both the state \mathbf{x} and its parameters \mathbf{p} are contained in the system dynamics. The augmented state vector \mathbf{x}' is then defined as:

$$\begin{aligned} \mathbf{x}'_{k+1} = \begin{bmatrix} \mathbf{x}_{k+1} \\ \mathbf{p}_{k+1} \end{bmatrix} &= \begin{bmatrix} f(\mathbf{x}_k) + g(\mathbf{x}_k) \mathbf{v}_k + \mathbf{w}_k \\ \mathbf{p}_k + \mathbf{w}_{pk} \end{bmatrix} = \\ &= f'(\mathbf{x}'_k, \mathbf{v}_k, \mathbf{w}_k, \mathbf{w}_{pk}) \end{aligned} \quad (9)$$

being \mathbf{w}_{pk} a artificial noise that allows the EKF to change the estimate of \mathbf{p}_k and $f(\mathbf{x}'_k, \mathbf{v}_k, \mathbf{w}_k, \mathbf{w}_{pk})$ a nonlinear function of the augmented state \mathbf{x}'_k .

To apply the above for jet engine parameter identification, we first discretize (7) and then extend the state with the parameter vector \mathbf{p} , namely:

$$\mathbf{x}'_{k+1} = \begin{cases} T_{k+1} &= T_k + \dot{T}_k \Delta t + \ddot{T}_k \frac{\Delta t^2}{2} \\ \dot{T}_{k+1} &= \dot{T}_k + \ddot{T}_k \Delta t \\ \mathbf{p}_{k+1} &= \mathbf{p}_k \end{cases} \quad (10)$$

where \ddot{T}_k is the second derivative (7) of the thrust evaluated at time instant k and Δt the sampling interval.

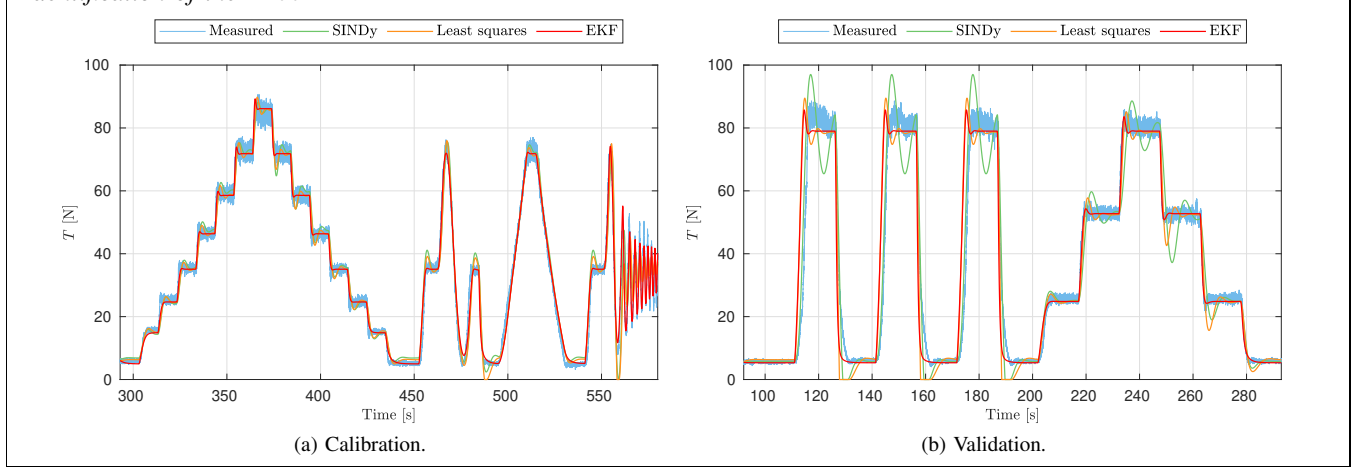
The EKF Algorithm 1 is then used to estimate the state $[T, \dot{T}, \mathbf{p}]^\top$. Since we are interested in estimating \mathbf{p} , we run procedure offline and on the collected datasets. The choices of the initial state guess, covariance error, and noise matrices are critical for the EKF tuning. In our case, the initial guess of \mathbf{p} influences considerably the overall results associated with the identification of \mathbf{p} . We solved this issue running iteratively the EKF algorithm on the dataset to improve, run by run, the initial guess, while performing a proper tuning of the matrices \mathbf{Q} , \mathbf{R} and \mathbf{P} .

C. Experimental results of the identification procedure

In this section, we show the results of the gray box identification procedures presented in Sec. V-A and V-B. We apply the procedures to identify the model parameters associated with the P100-RX and the P220-RXi jet engines. When testing the identification procedure based on the EKF, the variance of the noise measurement, namely \mathbf{Q} , is $\sim 7 \text{ N}^2$ for the P100-RX and $\sim 9 \text{ N}^2$ for the P220-RXi.

Fig. 6 shows the experimental data for calibration (left) and validation (right) purposes. Note that all three presented identification procedures are plotted both for the calibration and validation datasets. It is here clear how the EKF based identification procedure outperforms both SINDy and classical iterative least squares. As mentioned previously, this is believed to be the consequence of the intrinsic robustness of the EKF to measurement noise, and to its independence from noncausal filters to estimate higher order thrust derivatives. Table III shows the parameters identified by the three identification procedure. The results on the validation datasets are presented in Fig. 6b and 6d: the EKF method outperforms the other two methods. Table IV shows the mean square error obtained testing the model on 9 different datasets.

Identification of the P100-RX



Identification of the P220-RXi

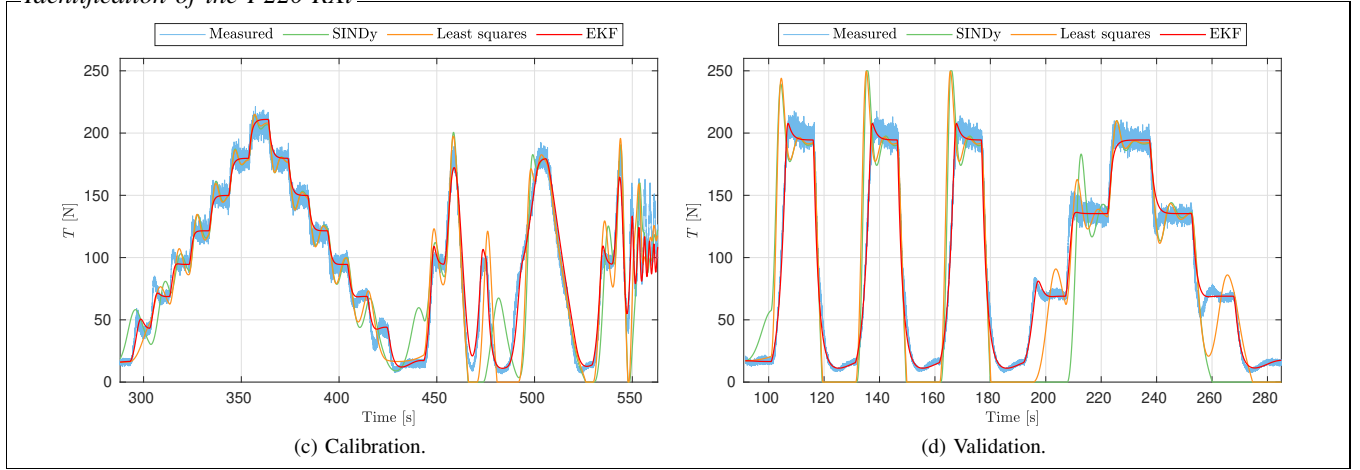


Fig. 6: Identification: calibration phase (a-c) and validation of the identified model (b-d).

Parameter	EKF		LS	
	P100-Rx	P220-RXi	P100-Rx	P220-RXi
K_T	-1.460	-0.280	-0.617	0.2027
K_{TT}	-0.059	-0.010	-0.015	-0.003
K_D	-2.430	0.5883	-0.737	-0.196
K_{DD}	0.0787	0.0421	-0.002	0.0023
K_{TD}	0.1188	0.0058	0.0020	-0.002
B_U	0.4317	0.1874	0.2175	-1.364
B_T	0.0116	0.0137	0.0090	-0.002
B_D	-0.026	-0.032	-0.001	0.0067
B_{UU}	0.0314	0.0074	0.0078	-0.015
c	-19.92	-7.839	-5.631	20.624

TABLE III: The identified parameters for both the turbines.

Jet turbine model	Mean square error		
	EKF	LS	SINDy
P100-RX	3.94 N	4.40 N	5.11 N
P220-RXi	6.77 N	13.41 N	21.34 N

TABLE IV: Mean square error on the validation dataset.

VI. CONTROL

In this section, we present strategies to control the model jet engines. We assume that the jet engine is described by the model (7), and that the control objective is the asymptotic stabilisation of a desired thrust force T_d .

A. Feedback Linearization control

In this case, the role of the control input u is to obtain a closed loop dynamics of the form:

$$\ddot{T} = \ddot{T}_d + K_p(T_d - T) + K_d(\dot{T}_d - \dot{T}) \quad (11)$$

where K_p and K_d are two positive constants. The control law that achieves this closed loop is given by:

$$v = \frac{\ddot{T}_d + K_p(T_d - T) + K_d(\dot{T}_d - \dot{T}) - f(T, \dot{T})}{g(T, \dot{T})} \quad (12)$$

then solving the equation $v = u + B_{UU}u^2$ we obtain our real turbine input u . Note that $u \in [25, 100]$ % by datasheet. In this interval the function $v = u + B_{UU}u^2$ must be positive and monotone, in order to take as solution the positive root.

B. Sliding mode controller

First, define the following error dynamics:

$$\begin{cases} \tilde{T} = T - T_d \\ \dot{\tilde{T}} = \dot{T} - \dot{T}_d \\ \ddot{\tilde{T}} = \ddot{T} - \ddot{T}_d, \end{cases} \quad (13)$$

which leads to:

$$\ddot{\tilde{T}} = f(T, \dot{T}) + g(T, \dot{T}) \cdot v(u) - \ddot{T}_d \quad (14)$$

The *sliding manifold* is then defined as:

$$s(\tilde{T}, \dot{\tilde{T}}) = a_1 \tilde{T} + \dot{\tilde{T}} \quad (15)$$

where a_1 is a positive constant. To further reduce the aggressiveness of the control law, we can substitute the switching component of (5), i.e. the $\text{sgn}(\cdot)$ function, with the continuous approximation $\tanh(\cdot) \in [-1, 1]$.

From (5) and (13), the control law is then:

$$v = -\frac{a_1 \dot{\tilde{T}} + (f(T, \dot{T}) - \ddot{T}_d)}{g(T, \dot{T})} - \beta \cdot \tanh(K \cdot s) \quad (16)$$

where K is an additional positive constant regulating the slope of the $\tanh(\cdot)$ function. We obtain our real turbine input u solving the equation $v = u + B_{UV}u^2$.

C. Control architecture

The only available measurement is the thrust magnitude T . We used an Extended Kalman Filter as state observer in order to retrieve the full state $[T, \dot{T}]$. The control architecture is depicted in Fig. 7.

D. Experimental results of the control architecture

In this section, we show the control performance of the feedback linearization and sliding mode controller on the model jet engine P100-RX.

Fig. 8 shows the performance obtained by applying the feedback linearization controller. Despite the fact that exact feedback linearisation methods in general lack robustness, the controller achieves acceptable tracking performances. The associated controller gains are shown in Table. V.

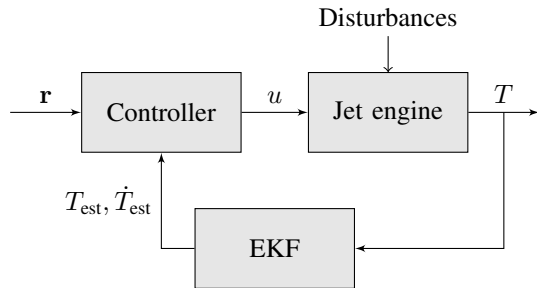


Fig. 7: The jet engine control architecture, $\mathbf{r} = [T_d, \dot{T}_d, \ddot{T}_d]^T$

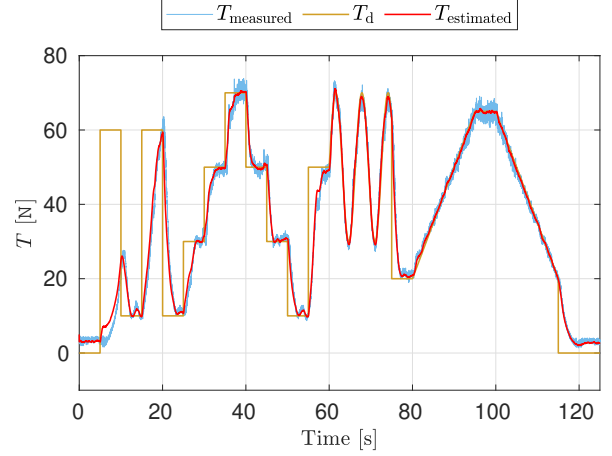


Fig. 8: Feedback linearization controller.

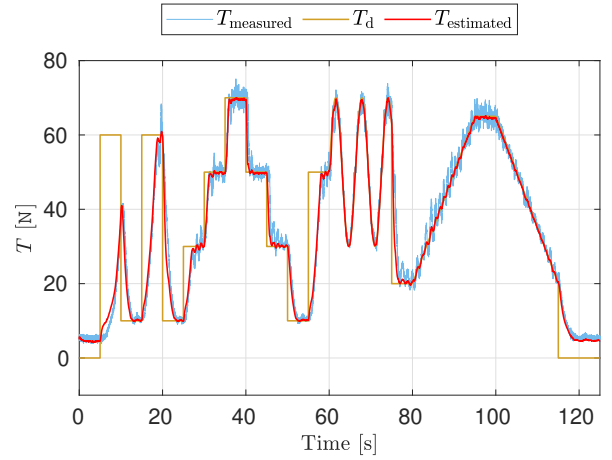


Fig. 9: Sliding mode controller.

Sliding Mode			Feedback Linearization	
a_1	β	K	K_p	K_d
20	900	0.15	10	$2\sqrt{K_p}$

TABLE V: Controllers gains.

Fig. 9 shows the behavior of the jet engine when controlled by the sliding mode controller. This control technique exerts a more aggressive control authority, causing an oscillation of the trajectory along the given reference.

The main critical point of the control architecture is the robustness with respect to the model uncertainties. Despite the use of "exciting" inputs during the identification phase, it may occur that not all the dynamics of the system are excited and, hence, identified. A typical case is the one relative to high-frequency dynamics.

An undesired phenomenon that could emerge with Sliding mode control is the so called *chattering*. Fig. 10 shows the effects of an high-frequency input produced by a *deliberately* not properly tuned Sliding mode control. The input excites unmodelled high-frequency dynamics of the jet engine, leading to a sensible performances degradation.

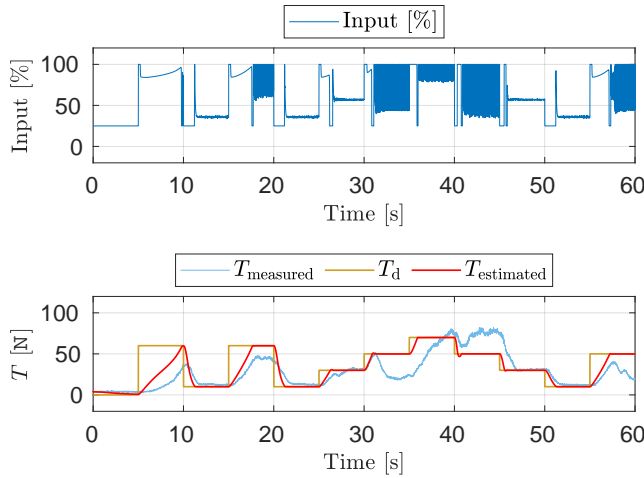


Fig. 10: An example of *chattering* phenomena (25 s - 60 s): an high frequency input excites unmodeled high frequency dynamics.

VII. CONCLUSIONS

This paper presents the first comprehensive approach to the modeling, identification and control of model jet engines, with experimental validation of the overall methodology.

Model jet engines are propulsion systems that are still not exploited in Robotics, and may open up to new robot design combining several degrees of manipulation and locomotion, as in the case of flying humanoid robots.

This work is based on the main assumption that the jet engines governing dynamics is described by a second order, nonlinear model. We used the sparse identification on nonlinear dynamics SINDy in order to find out the governing model, and then we addressed the identification problem is by means of a *gray-box* approach.

After system identification, we propose and validate nonlinear controllers for tracking a thrust reference. In particular, we presented feedback linearization and sliding mode controllers. The results show that the both the controllers are able to track the given reference, although the Sliding mode control is more sensitive to the gain tuning.

Future extension of this work include the design of MPC controllers, tacking into account the input limitation and the efficiency of the model jet engine; the development of a backstepping control technique in order to use the model jet engines on the iCub Flying Humanoid.

REFERENCES

- [1] C. F. Liew, D. DeLatte, N. Takeishi, and T. Yairi, "Recent developments in aerial robotics: A survey and prototypes overview," *CoRR*, vol. abs/1711.10085, 2017. [Online]. Available: <http://arxiv.org/abs/1711.10085>
- [2] F. Ruggiero, V. Lippiello, and A. Ollero, "Aerial manipulation: A literature review," *IEEE Robotics and Automation Letters*, vol. 3, no. 3, pp. 1957–1964, July 2018.
- [3] G. Heredia, A. E. Jimenez-Cano, I. Sanchez, D. Llorente, V. Vega, J. Braga, J. A. Acosta, and A. Ollero, "Control of a multirotor outdoor aerial manipulator," in *2014 IEEE/RSJ International Conference on Intelligent Robots and Systems*, Sep. 2014, pp. 3417–3422.
- [4] M. Pitonyak and F. Sahin, "A novel hexapod robot design with flight capability," in *2017 12th System of Systems Engineering Conference (SoSE)*, June 2017, pp. 1–6.
- [5] A. Bozkurt, A. Lal, and R. Gilmour, "Aerial and terrestrial locomotion control of lift assisted insect biobots," in *2009 Annual International Conference of the IEEE Engineering in Medicine and Biology Society*, Sept 2009, pp. 2058–2061.
- [6] A. Kalantari and M. Spenko, "Design and experimental validation of hytaq, a hybrid terrestrial and aerial quadrotor," in *2013 IEEE International Conference on Robotics and Automation*, May 2013, pp. 4445–4450.
- [7] L. Daler, S. Mintchev, C. Stefanini, and D. Floreano, "A bioinspired multi-modal flying and walking robot," *Bioinspiration & Biomimetics*, vol. 10, no. 1, p. 016005, 2015. [Online]. Available: <http://stacks.iop.org/1748-3190/10/i=1/a=016005>
- [8] L. Daler, J. Lecoeur, P. B. Hählen, and D. Floreano, "A flying robot with adaptive morphology for multi-modal locomotion," in *2013 IEEE/RSJ International Conference on Intelligent Robots and Systems*, Nov 2013, pp. 1361–1366.
- [9] "Caltech building agile humanoid robot by combining legs with thrusters," <https://spectrum.ieee.org/automaton/robotics/humanoids/caltech-building-agile-humanoid-robot-by-combining-legs-with-thrusters>, Feb 2019.
- [10] Z. Huang, B. Liu, J. Wei, Q. Lin, J. Ota, and Y. Zhang, "Jet-hr1: Two-dimensional bipedal robot step over large obstacle based on a ducted-fan propulsion system," in *2017 IEEE-RAS 17th International Conference on Humanoid Robotics (Humanoids)*, Nov 2017, pp. 406–411.
- [11] C. Bartolozzi, D. Pucci, A. Wykowska, and G. Metta, "icub: The not-yet-finished story of building a robot child," *Science Robotics*, vol. 2, 2017.
- [12] D. Pucci, S. Traversaro, and F. Nori, "Momentum control of an underactuated flying humanoid robot," *IEEE Robotics and Automation Letters*, vol. 3, no. 1, pp. 195–202, 2017.
- [13] G. Nava, L. Fiorio, S. Traversaro, and D. Pucci, "Position and attitude control of an underactuated flying humanoid robot," in *2018 IEEE-RAS 18th International Conference on Humanoid Robots (Humanoids)*. IEEE, 2018, pp. 1–9.
- [14] C. Hall and S. L. Dixon, *Fluid mechanics and thermodynamics of turbomachinery*. Butterworth-Heinemann, 2013.
- [15] Rolls Royce plc., *The jet engine*. Wiley, 2015.
- [16] S. L. Brunton, J. L. Proctor, and J. N. Kutz, "Discovering governing equations from data by sparse identification of nonlinear dynamical systems," *Proceedings of the National Academy of Sciences*, vol. 113, no. 15, pp. 3932–3937, 2016. [Online]. Available: <https://www.pnas.org/content/113/15/3932>
- [17] A. Isidori, *Nonlinear control systems*. Springer Science & Business Media, 2013.
- [18] H. K. Khalil and J. W. Grizzle, *Nonlinear systems*. Prentice hall Upper Saddle River, NJ, 2002, vol. 3.
- [19] Wikipedia, "Lithium polymer battery," 2019. [Online]. Available: https://en.wikipedia.org/wiki/Lithium_polymer_battery
- [20] —, "Diesel fuel," 2019. [Online]. Available: https://en.wikipedia.org/wiki/Diesel_fuel
- [21] "The "cat 6" fan," <https://edfdynamax.com/%22cat-6%22-plug%26play-system>.
- [22] "Jetcat p220-rxi," 2019. [Online]. Available: <https://www.jetcat.de/en/productdetails/produkte/jetcat/produkte/hobby/Engines/p220-rxi>
- [23] D. Simon, *Optimal state estimation: Kalman, H infinity, and nonlinear approaches*. John Wiley & Sons, 2006.
- [24] "Jetcat p100-rx," 2019. [Online]. Available: <https://www.jetcat.de/en/productdetails/produkte/jetcat/produkte/hobby/Engines/p100-rx>
- [25] P. Fitzpatrick, E. Ceseracciu, D. Domenichelli, A. Paikan, G. Metta, and L. Natale, "A middle way for robotics middleware," *Journal of Software Engineering for Robotics*, vol. 5, pp. 42–49, 2014.
- [26] F. Romano, S. Traversaro, D. Pucci, and F. Nori, "A whole-body software abstraction layer for control design of free-floating mechanical systems," *Journal of Software Engineering for Robotics*, 2017.